An ***ab initio*** study of muons in ethanal

1997 J. Phys.: Condens. Matter 9 3241

(http://iopscience.iop.org/0953-8984/9/15/015)

J. Phys.: Condens. Matter **9** (1997) 3241–3257. Printed in the UK PII: S0953-8984(97)76641-4

An *ab initio* study of muons in ethanal

M I J Probert† and A J Fisher

Department of Physics and Astronomy, University College London, Gower Street, London WC1E 6BT, UK

Received 25 July 1996, in final form 10 February 1997

Abstract. *Ab initio* density functional theory calculations for ethanal and muonium, using the projector augmented-wave technique, are described. The potential binding sites for the muonium are evaluated from total-energy-minimization calculations. At these preferred sites the associated (bond-stretching) vibrational frequencies, Einstein coefficients and isotropic hyperfine coupling constants are then calculated. It is found that the hyperfine parameter at each site depends on the vibrational state, and so muon vibrational spectroscopy of ethanal is predicted to be possible. The effect of a rigid-muonium-bond rotation is also considered. It is found that this can change the sign of the predicted hyperfine coupling constant at certain sites, which is necessary to get reasonable agreement with experimental values. The temperature dependence of the hyperfine coupling constant was calculated from a Boltzmann population of rotational states. This was found to be insufficient to explain the experimentally observed temperature dependence. This is probably due to the neglect of coupling between vibrational and rotational modes. Therefore this common interpretation of the experimental temperature dependence of the hyperfine coupling constant must be reconsidered.

1. Introduction

1.1. Background

A new application of the muon spin rotation (μSR) technique has recently been proposed [1], in which the basics of a new technique, that of muon vibrational spectroscopy, were outlined. The essence of the technique is to illuminate a sample in a μSR experiment with light at an appropriate frequency to cause vibrational excitation of the atomic muonium bond, and detect the existence of this excitation from the change in the hyperfine coupling constant measured from the μSR spectrum. To our knowledge, the proposed experimental technique has never been tested, and so there was a need for a 'proof of principle' study of this proposal. This we reported in a recent paper [2], on the basis of a set of *ab initio* calculations of benzene. Benzene was chosen as it was computationally simple and the benzene ring is a structural motif that occurs widely in the organic compounds that would be most widely studied by this technique.

There is considerable interest in performing such experiments, with benzophenone ($C_6H_6COC_6H_6$ as in figure 1(a)) being a promising initial candidate material, as it can be grown in well-characterized crystals. The use of a crystalline material would simplify the experiment by eliminating solvent effects. Benzophenone can be considered as two benzene rings, joined by a carbonyl group. As we have already reported the results of

† Current address: Department of Physics, Cavendish Laboratory, University of Cambridge, Madingley Road, Cambridge CB3 0HE, UK.

0953-8984/97/153241+17$19.50

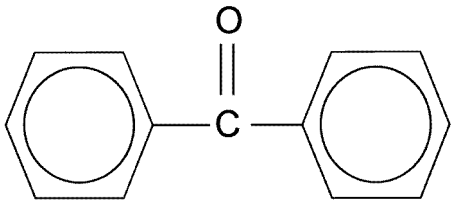

(a)

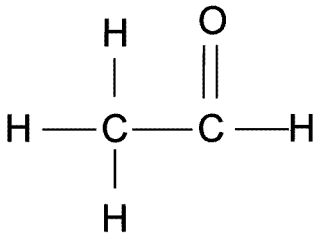

(b)

Figure 1. Chemical structure of (a) benzophenone and (b) ethanal.

a study of benzene, we shall in this paper consider the properties of the carbonyl group. Instead of considering the benzophenone molecule, we shall study the computationally simpler molecule of ethanal (CH_3CHO; figure 1(b)). Ethanal shares the same carbonyl group as the more complex benzophenone, and the bonding sites of muonium in ethanal and benzophenone are expected to be very similar. Previous μSR experiments on benzophenone have suggested that the muonium only bonds to the carbonyl site [3]. Ethanal is also a useful test molecule, as there have already been μSR studies of ethanal [4, 5] against which we can compare our predictions. Unfortunately, ethanal is a liquid at normal temperatures and pressures and is therefore subject to solvent effects. In this study, we ignore such effects by considering only a single molecule in isolation at zero temperature. Thermal effects will be included, where appropriate, by a Boltzmann population of excited vibrational or rotational states.

1.2. Motivation

One of the principal motivations for the μSR technique is that the implanted positive muon often forms muonium (μ^+e^-) which can be used as a hydrogen substitute, forming bonds, defect centres, etc, and as such has found many uses as a probe of condensed matter [6]. The proposed muon vibrational spectroscopy would extend the range of phenomena that could be investigated. However, the technique is quite experimentally intricate, and as such would benefit considerably from some reliable predictions to guide the experimental design and operation. In particular, there is a need to know the vibrational frequencies to be excited, the lifetime of the excited states, and the corresponding change in the hyperfine coupling constants. We have decided to concentrate on the bond-stretching modes, as simple predictions based on the ratio of the mass of muonium and hydrogen suggests that the bond-stretching modes are expected to be ideally local, with no other modes nearby in frequency. Bond-bending modes will be considerably lower in frequency and are therefore likely to

couple to other phonon modes.

The detection of molecular vibrations in conventional molecules is a standard way to determine molecular structures and properties. It is widely used in organic chemistry to identify the structural groups present, and their bond strengths and lengths. The following question then arises: if muonium can behave as a hydrogen atom and form chemical bonds, how can its vibrational states be detected? An obvious problem is that in a typical μSR experiment there is only a very low density of muons in the sample at any one time—typically 10^3—compared to $\sim 10^{23}$ molecules. Therefore the proportion of muonated bonds to normal bonds will be vanishingly small and extremely difficult to detect by conventional absorption techniques. However, if some signature could be found that depended only on the muons or their decay products, then such an experiment might be possible. It was proposed [1] that such a signature would be the change in the hyperfine coupling constant. In a recent paper [2] we therefore simulated a μSR experiment of benzene and predicted the change in hyperfine coupling constant upon vibrational excitation. This we predicted should be experimentally verifiable as the vibrational state was found to be metastable, with a lifetime comparable to that of the muon.

The implanted muons in a μSR experiment form muonium by acquiring an electron once they have lost sufficient energy. This hydrogen-like atom has much greater zero-point motion than hydrogen, owing to the much lighter mass of the muon ($\sim 1/9$ proton mass). The electronic states of muonium are hydrogen-like, with a 1s ground state that is split by the hyperfine (magnetic) interaction of the electron spin $\boldsymbol{S}$ and muon spin $\boldsymbol{I}$. This splitting is proportional to the electron spin density at the muon, and gives rise to the isotropic hyperfine coupling constant, $A_\mu \sim |\Psi(0)|^2$, which is usually expressed as a frequency. Vacuum-state muonium has $A_\mu \sim 4.5$ GHz which is greater than that for a hydrogen atom by the approximate ratio of the magnetic moment of the muon to that of the proton, confirming the description of muonium as a pseudo-isotope of hydrogen. The hyperfine coupling constant is however sensitive to the local environment, and is often lower for muonium in a host material than in a vacuum, corresponding to some delocalization of the electronic wavefunction onto the neighbouring atoms. It can be measured in a zero-field μSR experiment as the muon-spin-precession frequency, or by the repolarization technique [7, 8] in a longitudinal field.

In this paper we simulate a μSR experiment on ethanal as a guide to the real experiments on benzophenone. The behaviour of muonium in ethanal is more complex than in benzene, as there are now multiple possible binding sites, and the carbonyl group is more chemically reactive than the benzene ring. In section 2 we briefly outline the essential theory underlying the simulations, being both standard density functional theory and the less-well-known projector augmented-wave method. In section 3 we give some details of the actual methodology used, with the results and accompanying discussion following in section 4. This is broken down into the calculation of equilibrium properties, then vibrational excitations, and finally rotational excitations. Final conclusions are summarized in section 5.

2. Theoretical background

2.1. Density functional theory

The calculations were performed using an *ab initio* technique based on density functional theory (DFT) [9, 10], within the local spin-density (LSD) approximation. We used the recently developed projector augmented-wave (PAW) method [11] rather than a conventional pseudo-potential method as it is an all-electron method, having several key features

necessary for these calculations. Firstly, being an all-electron method it is capable of handling the light first-row elements necessary for organic compounds, where conventional pseudo-potentials have difficulty (particularly with oxygen). Secondly, as it works with the full valence electron wavefunction, it can be used to calculate such quantities as the net electronic spin density at the nucleus, which is necessary for calculating the hyperfine coupling constant. Finally, the method can be used for both energy minimization and also molecular dynamics using the Car–Parrinello [12] algorithm.

The basic theorems of density functional theory are that the ground-state energy of a system is a functional of the ground-state electron density, and that this energy can be found by minimizing the appropriate functional. In this way, it is possible to work with the electron density rather than the full many-body wavefunction, which is a great saving in computational complexity. The electron density $\rho(\boldsymbol{r})$ can be expressed as a sum over single-electron wavefunctions, $\rho(\boldsymbol{r}) = \sum_\mu |\chi_\mu|^2$, which are not themselves directly related to the many-body wavefunction. These single-electron wavefunctions are often expanded in a basis of plane waves, and are found by solving the Kohn–Sham equations [10] in a self-consistent manner. Most implementations of DFT replace the ionic potential with a pseudo-potential, in which the details of electronic structure are smoothed out within a certain core radius. This has the advantage of computational efficiency if the only quantities of interest are those that depend on the electron density at a reasonable distance from the atomic core. However, this approach has great difficulty with first-row elements, where the 2p orbitals are very compact and therefore require a large number of plane waves for the expansion to converge.

2.2. The projector augmented-wave method

The PAW method is an 'all-electron' method, and as such goes beyond the pseudo-potential method, although both the 'ultra-soft' pseudo-potential method of Vanderbilt [13] and the 'linear augmented-plane-wave' (LAPW) method [14] can be derived from it in appropriate limits. In the PAW method, the all-electron wavefunction $|\psi_{AE}\rangle$ for a given site is given by a smooth pseudo-wavefunction plus a one-centre correction:

$$|\psi_{AE}\rangle = |\tilde{\psi}\rangle + \sum_i (|\phi_i\rangle - |\tilde{\phi}_i\rangle)\langle\tilde{p}_i|\tilde{\psi}\rangle \tag{1}$$

where the one-centre correction is the difference between two localized 'partial waves', and $|\tilde{p}_i\rangle$ is a 'projector function'. The pseudo-partial wave, $\sum_i c_i|\tilde{\phi}_i\rangle$, only exists within some augmentation sphere, of radius $\Omega_{\boldsymbol{R}}$ centred on each atom, and is equal to the pseudo-wavefunction within this radius. The all-electron partial wave, $\sum_i c_i|\phi_i\rangle$, again only exists within a radius $\Omega_{\boldsymbol{R}}$ centred on each atom, and is equal to the full single-electron wavefunction within this radius. The pseudo-wavefunction $|\tilde{\psi}\rangle$ is smooth and exists over all space. The coefficients c_i are obtained by the use of the projector functions within the augmentation sphere. There may be more than one such projector function per angular momentum state, and these functions are constructed to be orthonormal to the corresponding pseudo-partial waves. The pseudo-wavefunction is expressed in terms of plane waves, whereas both the pseudo- and all-electron partial waves are expressed as products of radial functions and spherical harmonics on a radial grid, centred on each atom. Full details of the calculation of these projectors can be found in the original paper [11]. The net result is a generalized separable form of the ionic potential, which can be either norm conserving or non-norm conserving as required. This potential can then be used for Car–Parrinello-like dynamics or energy minimization.

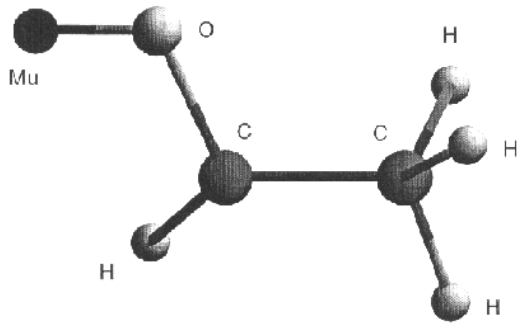

(a)

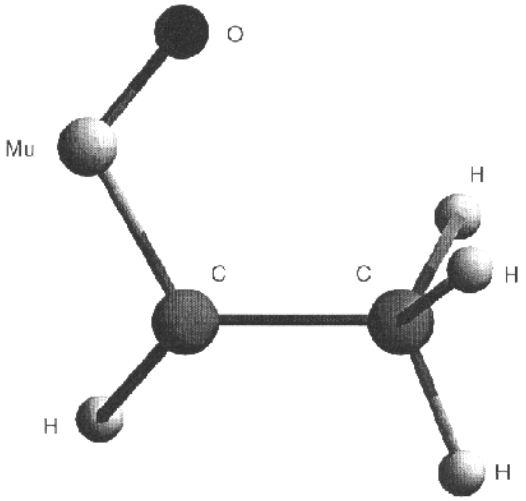

(b)

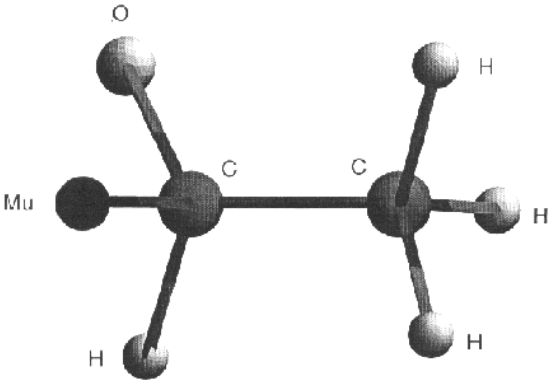

(c)

Figure 2. Equilibrium structure of ethanal with a muonium atom bonded in the three stable positions: (a) bonded to the oxygen atom in the *trans*-conformer, (b) bonded to the oxygen atom in the *cis*-conformer, (c) bonded to the carbon atom.

All other quantities of interest are expressed in a similar fashion. In particular, the all-electron charge density is given by

$$\rho(\boldsymbol{r}) = \tilde{\rho}(\boldsymbol{r}) + \rho^1(\boldsymbol{r}) - \tilde{\rho}^1(\boldsymbol{r}) \tag{2}$$

where $\tilde{\rho}(\boldsymbol{r})$, $\rho^1(\boldsymbol{r})$, $\tilde{\rho}^1(\boldsymbol{r})$ are the charge densities associated with the pseudo-wavefunctions, all-electron partial waves, and pseudo-partial waves respectively, and each contains the contribution of their respective core states. Similar expressions for the spin density can be derived, and in particular, as this is an all-electron method, the electron spin at the ionic nucleus can be found, which is an essential parameter for the calculation of hyperfine coupling constants.

3. Method

3.1. Calculation of equilibrium structures, vibrations and rotations

We used the PAW method with damped dynamics to perform total energy minimizations, in order to evaluate the most likely candidate binding sites of the muon and calculate which of the possible structures are energetically stable. We then performed a direct simulation of the muonium vibrations using undamped dynamics, with all of the atoms free to move and the muonium displaced by a small amount (0.1 au) from its equilibrium position. In this way we were able to calculate vibrational frequencies directly in the classical approximation. From this we found that the amplitude of the zero-point vibration is large, which was expected because of the very low mass of the muonium atom. Within the PAW technique we treat the muonium as a light pseudo-isotope of hydrogen. The motion of the muonium ion is therefore treated with classical mechanics using forces derived from the PAW energy functional, and does not fully capture all of the features of the quantum zero-point motion.

We then calculated the expectation values of the hyperfine coupling constant for the different binding sites, for both the ground state and first vibrationally excited states, by a sequence of energy-minimization calculations along the bond-stretch direction. The energy surface is anharmonic over these larger displacements from equilibrium, and so perturbation theory was used to calculate appropriate vibrational wavefunctions and expectation values. We then repeated this procedure for a 2π-rotation of the muonium bond about the carbon–oxygen axis, calculating the rotational energy levels and expectation values for the hyperfine coupling constant.

3.2. Technical details of the calculations

Calculations were performed with the spin-polarized PAW method on a single molecule of ethanal plus a muonium atom in a box of size $(10\ \text{au})^3$ at zero temperature. A plane-wave basis set was used for the wavefunctions, with a 30 Ryd cut-off in order to get a good description of the oxygen atom. A single projector was used for the hydrogen and muonium atoms, whilst two projectors were used for each carbon atom, with norm conservation. For the oxygen atom it was found that a four-projector non-norm-conserving potential was required, in order to get a well-converged result within the 30 Ryd plane-wave cut-off.

4. Results and discussion

4.1. Equilibrium structures

Various possible bonding positions for the muon were considered, and the total energy of the system was minimized as each of these structures was relaxed. Three of these sites proved to be stable and form the basis of the results presented herein. Two of these configurations correspond to the muonium bonding to the oxygen atom, in *trans*- and *cis*-positions. The other corresponds to the muonium bonding to the unsaturated carbon atom, as seen in figures 2(a)–2(c). Other possible sites, such as binding to any of the hydrogen atoms or the methyl group carbon atom, proved to be unstable.

Table 1. Results from static energy-minimization calculations. Typical sampling errors in each quantity are given in the first row of the table.

Site	Binding energy (eV)	Bond length (au)	Bond length (Å)
trans-oxygen	4.85 ± 0.02	1.859 ± 0.004	0.984 ± 0.002
cis-oxygen	4.93	1.890	1.000
Carbon	4.58	2.210	1.169

The binding energies were calculated by comparing the total energy of the muonium-bonded system with the sum of the energy of an ethanal molecule and that of an isolated muonium atom in a box of the same size and with the same basis sets. This showed that the most stable configuration was that with the muonium bonded to the oxygen atom in the *cis*-position, followed by the oxygen *trans*-conformer, and finally the bonding to the carbon atom. The results for these calculations are summarized in table 1. It should be noted that there is a large structural difference between the configurations with muonium bonded to oxygen and to carbon. In the oxygen configurations, the unsaturated carbon atom is in an sp^2 planar configuration, as in the original ethanal molecule, but when the muonium bonds to the carbon atom, this changes to an sp^3 tetrahedral configuration. The size of the binding energy in each case is in general agreement with that predicted from the energy of bond formation of O–H (4.8 eV in H_2O) and C–H (4.5 eV in CH_4) as in standard chemical tables [15], with the oxygen bond being the stronger as expected. It should be noted that previous *ab initio* simulations [5] based on the Hartree–Fock approach only considered the oxygen binding sites, and found that the two conformers were very similar in energy, with the *trans*-conformer being 0.002 eV more stable.

4.2. Dynamical calculation of bond-stretching vibrations

For each stable configuration, the muonium bond-stretching vibrational frequency was calculated by displacing the muonium atom from its equilibrium position by 0.1 au in the bond direction (to prevent any bond-bending modes being started), and then simulating the undamped dynamics of the system for about 50 fs. Care was taken in the choice of simulation time step (0.5 au) and fictitious electron wavefunction mass (2.5 au) to ensure adiabaticity of the Car–Parrinello dynamics [16] and prevent any energy transfer between atomic and electronic modes. This was necessary as the vibrational frequency would otherwise overlap the lower electronic modes. The mass preconditioning scheme [17] was used to compress the electronic modes and therefore increase the maximum time step. It was found that the bond-stretching motion of the muonium, for each configuration, occurs

in a frequency window (near infra-red), being considerably above any other atomic modes, and, with an appropriate choice of the fictitious mass of the electron wavefunctions, can be considerably below any electronic frequencies. This means that it should be possible to excite the mode in isolation. It should be noted that although the probability of populating a vibrational state by thermal excitation is negligible, there is the possibility that these states may be populated by the trapping of a muonium atom before it has reached thermal equilibrium. It is possible therefore that the effects discussed herein may already have been seen in previous conventional μSR experiments, but interpreted instead as a distribution of muonium bonding sites.

Table 2. Results from small-amplitude vibrational dynamics. Typical sampling errors in each quantity are given in the first row of the table.

Site	Frequency (THz)	Frequency (cm^{-1})	Einstein A (10^4 s^{-1})	Spontaneous lifetime (μs)	Einstein B (10^{18} J^{-1} m^3 s^{-1})	Laser PSD* (W GHz^{-1})
trans-oxygen	299 ± 5	9250 ± 180	35 ± 3	2.82 ± 0.06	19.2 ± 1.1	0.062 ± 0.06
cis-oxygen	288	8620	8.1	12.3	5.5	0.022
Carbon	206	6190	7.8	12.7	14.5	0.018

*This is the estimated power spectral density incident on a 1 cm^2 sample required to cause a 10% population of the first excited state.

The accuracy of these vibrational frequencies was checked by performing an identical dynamical calculation for the O–H bond stretch in ethanol and comparing to the established experimental value. This showed that LSD approximation was underestimating these frequencies by about 10% which can therefore be used as a guide to the systematic errors in the calculations. The results for these calculations are shown in table 2.

4.3. Optical properties of the bond-stretching vibrations

The Einstein A- and B-coefficients for optical excitation of the vibrational state were then calculated to see whether optical excitation will be experimentally feasible. The method used here was to calculate the electric dipole moment of the system, and its gradient tensor, from the electronic charge density for a series of small displacements in the muonium position about equilibrium. This was then used with the SHO assumption for the transition matrix elements to calculate values for the Einstein A- and B-coefficients. These results are included in table 2. As the vibration occurs in a frequency window, it seems quite reasonable to neglect non-radiative decay modes. Hence it can be seen from the Einstein A-coefficients that the vibrational states are reasonably metastable and will live for a significant fraction of the muon lifetime ($\tau_\mu \sim 2.2$ μs). This is another essential feature for the feasibility of the proposed experiment. The lifetime of the vibrationally excited *trans*-state is considerably shorter than that of the *cis*-state, because of the increased electric dipole moment caused by the muonium atom at a larger distance from the centre of charge for the rest of the molecule.

The Einstein B-coefficient can be used to give a guide to the amount of laser power required to excite the transition. If we assume a typical sample area of 1 cm^2 we can predict the required input power spectral density to achieve a 10% excitation at the appropriate frequency. This power density is also included in table 2. For a simple demonstration that the experiment works, the sample could be illuminated by a broad-band source, e.g., a Xe flashlamp, but for more quantitative studies the sample could be illuminated by a suitable IR laser, e.g., Ti:sapphire pumped with an Ar-ion or Cu-vapour source.

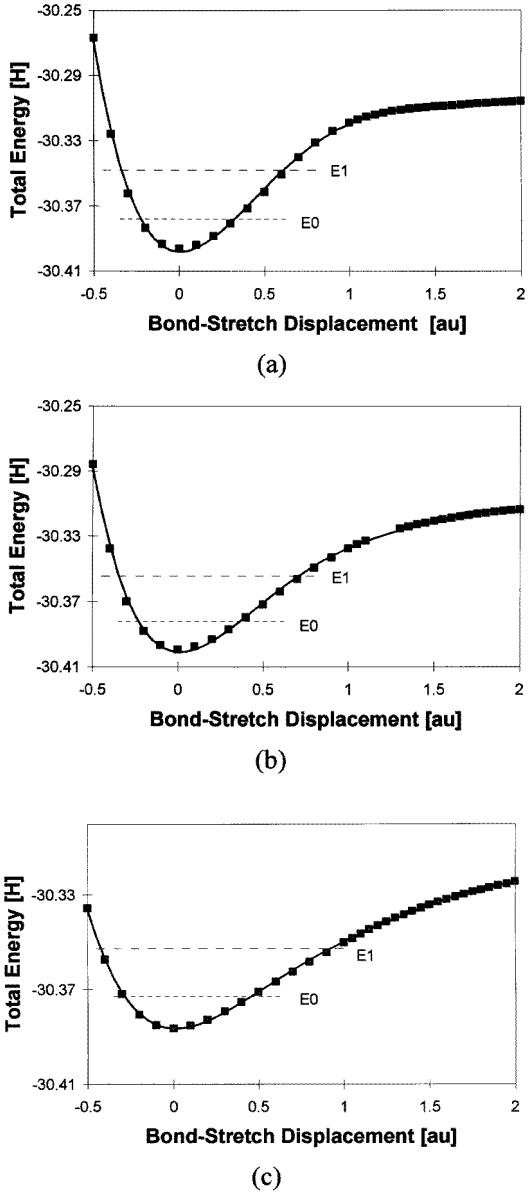

Figure 3. The total energy surface as a function of the muonium bond stretch about the equilibrium geometry for (a) the *trans*-oxygen site, (b) the *cis*-oxygen site, and (c) the carbon site. The squares correspond to measured energies from the simulation and the solid line is a fit to the data. The labelled dotted lines are the ground-state (E_0) and first-excited-state (E_1) vibrational energies obtained from the fit.

4.4. Static calculation of vibrational expectation values

The calculated (small-amplitude) vibrational frequencies were then used to make an estimate of the width of the muonium wavefunction within the SHO approximation. This 'width' was $\sim$1 au, which meant that the muonium wavefunction extended considerably beyond the

Table 3. Results from large-amplitude bond stretching. Typical sampling errors in each quantity are given in the first row of the table.

Site	g (anharmonicity)	A_μ (MHz) Equilibrium position	A_μ (MHz) Ground state	A_μ (MHz) First excited state
trans-oxygen	-0.07745	-23.1 ± 0.4	-25.1 ± 0.4	$+44.9 \pm 0.8$
cis-oxygen	-0.07828	21.9	64	225
Carbon	-0.07675	536	631	1020

0.1 au displacement treated so far. Therefore we stretched the muonium bond by a large amount and simulated the time evolution of the resulting state with undamped dynamics. However, because of the complex nature of the energy surface around the oxygen and carbon atoms, this sometimes resulted in a flipping of the muonium between bonding to the oxygen and the carbon atoms, and so the dynamical calculation was replaced by a sequence of static energy minimizations along the bond-stretch direction. The resulting potential energy surface for each site is shown in figures 3(a)–3(c), and the degree of anharmonicity was measured by fitting this to a cubic polynomial. This was then used with first-order perturbation theory, as in equation (3), to calculate approximate wavefunctions for the ground state and first vibrationally excited state:

$$H = H_{SHO} + \gamma x^3. \tag{3}$$

The degree of anharmonicity was characterized by the dimensionless parameter g:

$$g = \frac{\gamma}{\hbar\omega}\left(\frac{\hbar}{2m\omega}\right)^{3/2} \tag{4}$$

whose small values (see table 3) showed that first-order perturbation theory was quite sufficient to describe the resulting states. The effect of anharmonicity on the vibrational frequencies calculated from the small displacements is small (comparable to the other sources of error), and therefore is not included in the tabulated results.

The net electronic spin density at the muon was also measured, and used to calculate a value for the isotropic hyperfine coupling constant (A_μ) as a function of displacement from the equilibrium position. This is shown for each site as figures 4(a)–4(c). This was then used with the calculated vibrational wavefunctions to calculate an expectation value for A_μ in the ground state and first vibrationally excited state, for each of the stable muonium configurations. This shows that there is a significant increase (at least 70 MHz) in A_μ on excitation to the first vibrationally excited state, which should be clearly detectable in the proposed vibrational spectroscopy experiment. These values are shown in table 3.

These estimates for A_μ may be compared with the known experimental result of $A_\mu = 23$ MHz at ambient temperature [4]. This shows that for the energetically preferred *cis*-conformer, the vibrational ground-state average overestimates the electron spin density at the nucleus. For the *trans*-conformer, the predicted value is very close in magnitude to the experimental value, but of the wrong sign. The sign of A_μ is experimentally determined by the temperature dependence. There has been no report in the literature of a secondary, much higher value of A_μ, corresponding to the carbon site. The discrepancy between these predictions for A_μ and the experimental value may be due to the neglect of other zero-point motions (such as bond-bending modes) or due to the errors in the LSD approximation. Although the predictions may therefore be subject to significant errors, it is expected that the observed trend will still hold—that is, of a large increase in A_μ on vibrational excitation. The results for these calculations are summarized in table 3.

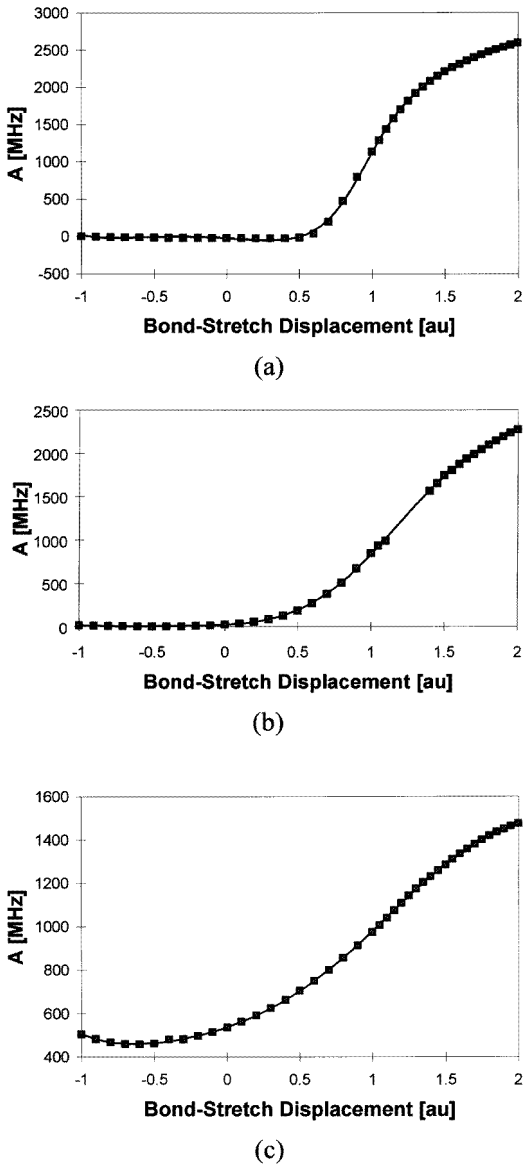

Figure 4. The hyperfine coupling constant as a function of the muonium bond stretch about the equilibrium geometry for (a) the *trans*-oxygen site, (b) the *cis*-oxygen site, and (c) the carbon site. The squares correspond to measured energies from the simulation and the solid line is a fit to the data.

A detailed temperature study of A_μ [5] has shown that there is a marked increase in A_μ with temperature. This was interpreted in terms of the excitation of rotational states, which have not so far been considered in this paper. A Hartree–Fock calculation [5] suggested that the spin density at the equilibrium position of the muon (and therefore the hyperfine coupling constant) was negative. It was therefore suggested that the observed positive value was due to hyperconjugation, with some of the spin density from the unpaired $2p_z$ orbital

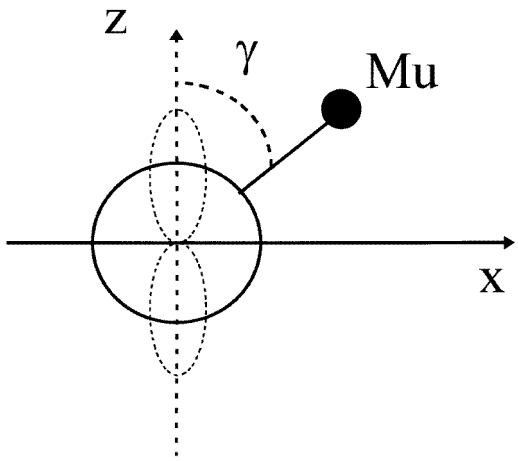

Figure 5. A schematic diagram showing the system of axes used to describe the muonium rotation. The C–O bond is parallel to the y-axis (out of the page) and the unpaired carbon p_z orbital defines the z-axis. The angle γ is defined as the angle between the z-axis and the projection of the O–Mu bond onto the xz-plane.

of the carbon atom appearing on the muon. This would be strongly dependent on the angle 'γ' of the oxygen–muonium bond to the direction of the carbon p_z orbital, as shown in figure 5, with the maximum spin-density transfer occurring when the orbitals are eclipsed, i.e. when $\gamma = 0$. Zero-point fluctuations in this angle about the equilibrium value ($\gamma = 90^\circ$) could then contribute a positive value to A_μ resulting in the observed value, which should be strongly temperature dependent. Measurements of $A_\mu(T)$ were fitted to a Boltzmann population of excited rotational states, where the rotational barrier is assumed to be of a simple twofold form:

$$V(\theta) = \tfrac{1}{2}V_2(1 - \cos(2\theta)). \tag{5}$$

It was assumed that the expectation value of A_μ for a given rotational state $|i\rangle$ is given by the Heller and McConnell form [18]

$$\langle A_\mu(\gamma)\rangle_i = L + M\langle\cos^2(\gamma)\rangle_i \tag{6}$$

with $\gamma = \theta - \theta_0$, where θ_0 is the value of θ at the minima of the energy barrier. L, M and V_2 are obtained from a least-squares fit to the experimental data. With this procedure, values of $L = -117.4$ MHz, $M = 298.4$ MHz and $V_2 = 0.0307$ eV were obtained [5].

We therefore decided to simulate the effect of rotation directly, and test how this affected the predictions for the hyperfine coupling constant and the temperature dependence.

Table 4. Results from a bond rotation of 2π.

Site	A_μ (MHz) Equilibrium position	$\langle A_\mu\rangle_0$ (MHz) Ground state	$\langle A_\mu(T)\rangle$ (MHz) at $T = 300$ K
trans-oxygen	−23.1	29.5	27.0
cis-oxygen	21.9	48.1	48.7

Table 5. Rotational states from a bond rotation of 2π.

Rotational state $\|i\rangle$	*trans*-oxygen Eigenenergy (eV)	*trans*-oxygen $\langle A_\mu \rangle_i$ (MHz)	*cis*-oxygen Eigenenergy (eV)	*cis*-oxygen $\langle A_\mu \rangle_i$ (MHz)
0	0.057	29.5	0.062	48.1
1	0.060	19.8	0.151	31.6
2	0.147	130.9	0.173	120.3
3	0.176	82.1	0.238	125.2
4	0.216	149.1	0.260	137.6

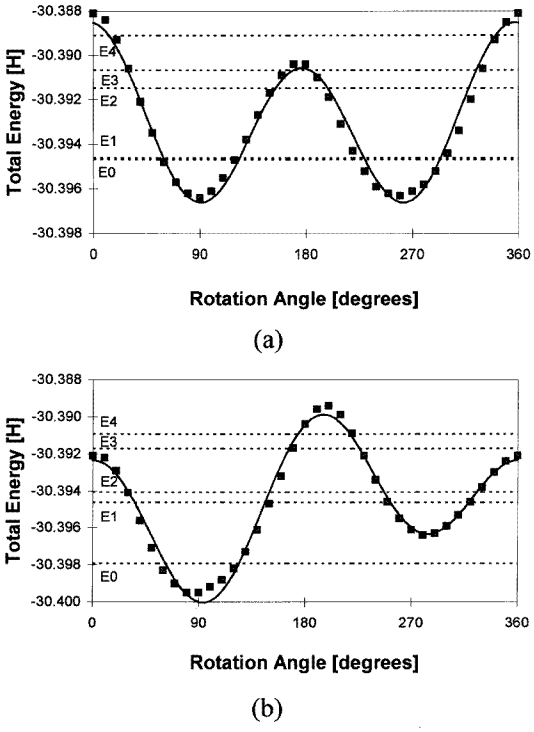

Figure 6. The total energy surface as a function of the rotation angle of the muonium atom, starting from (a) the *trans*-oxygen site and (b) the *cis*-oxygen site. The squares correspond to measured energies from the simulation and the solid line is a fit to the data, with the form of equation (7). The labelled dotted lines are the ground-state (E_0) and excited-state (E_1–E_4) rotational energies obtained from the fit as discussed in section 4.5.

4.5. Static calculation of rotational expectation values

From the equilibrium structures it can be seen that the *cis*- and *trans*-conformers have very similar O–Mu bond lengths (0.984 Å and 1.000 Å) and C–O–Mu bond angles (110.9° and 112.4°), which seemed to suggest that the two configurations correspond to the two minima in the rotational potential. We therefore performed a series of energy-minimization calculations of a rigid rotation of the O–Mu bond about the C–O axis. The bond angle (as in figure 5) was increased in 10° intervals at fixed bond length, whilst maintaining all other atoms in their equilibrium configuration. This was performed twice, once for each O–Mu

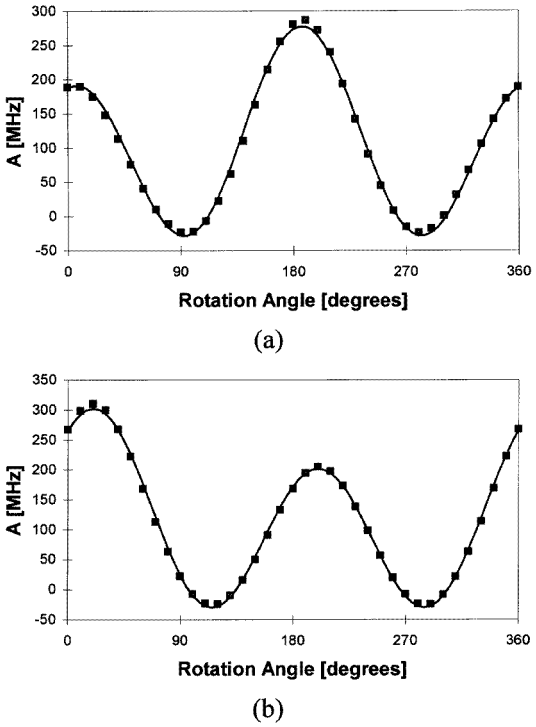

Figure 7. The hyperfine coupling constant as a function of rotation angle of the muonium atom, starting from (a) the *trans*-oxygen site and (b) the *cis*-oxygen site. The squares correspond to measured energies from the simulation and the solid line is a fit to the data.

conformer. At the end of each calculation, the hyperfine coupling constant was calculated. The resulting energy barriers are shown in figures 6(a) and 6(b), and the corresponding variation in A_μ with rotation angle is shown in figures 7(a) and 7(b). From figure 6 it can be seen that the simple form for the rotational barrier (equation (5)) is not sufficient, and the more general form

$$V(\theta) = V_0 + V_1 \cos(\theta - \theta_1) + V_2 \cos(2(\theta - \theta_2)) \tag{7}$$

was therefore used. A similar general form was also used to fit $A_\mu(\gamma)$. This rotational barrier was then used with the torsional Hamiltonian

$$H(\theta) = -\left(\frac{\overline{h}^2}{2I}\right)\frac{\delta^2}{\delta\theta^2} + V(\theta) \tag{8}$$

(where I is the moment of inertia), to calculate the corresponding eigenfunctions and energy eigenvalues. Each rotational eigenfunction was expanded in terms of a truncated plane-wave basis:

$$|\psi_i\rangle = \sum_m c_m^i |\varphi\rangle \qquad |\varphi_m\rangle = \frac{1}{\sqrt{2\pi}} \mathrm{e}^{\mathrm{i}m\theta} \tag{9}$$

with $m = -10$ to $+10$ being sufficient to give fully converged results for the low-lying levels of interest. The matrix elements of the Hamiltonian are therefore given by

$$H_{m,m'} = \left(\frac{\overline{h}^2 m^2}{2I} + V_0\right)\delta_{m-m'} + \tfrac{1}{2}V_1 \mathrm{e}^{\mp \mathrm{i}\theta_1}\delta_{m\pm 1-m'} + \tfrac{1}{2}V_2 \mathrm{e}^{\mp \mathrm{i}\theta_2}\delta_{m\pm 2-m'} \tag{10}$$

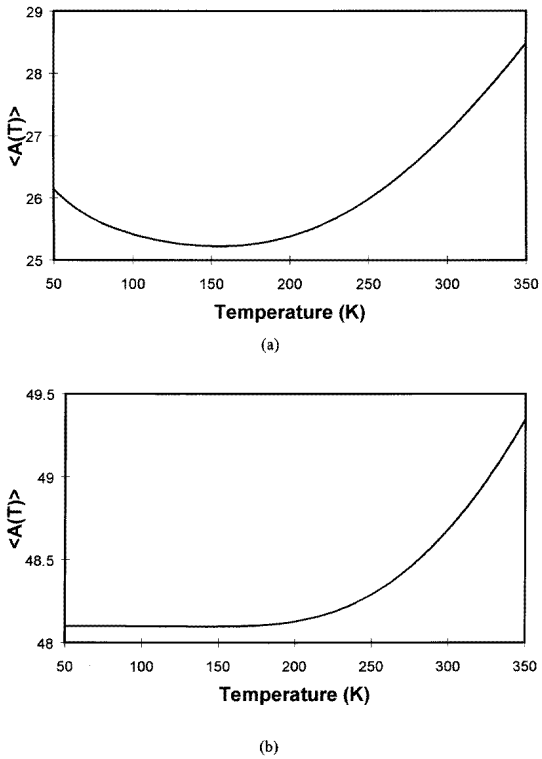

Figure 8. The predicted variation in hyperfine coupling constant with temperature from the Boltzmann population of rotational states, for (a) the *trans*-conformer site and (b) the *cis*-conformer site.

and a similar form may be used to express A_μ as an operator. Once the expansion coefficients c_m^i for each eigenfunction were known, expectation values of $\langle A_\mu \rangle_i$ were calculated. The rotational levels were then populated according to Boltzmann statistics at any given temperature, to give the corresponding thermal average $\langle A_\mu(T) \rangle$ as shown in figures 8(a) and 8(b). These results are summarized in table 4, whilst the individual eigenenergies and $\langle A_\mu \rangle_i$ are detailed in table 5.

The predicted value for $\langle A_\mu(300) \rangle$ is very close to the observed value of 23 MHz at ambient temperature [4] for the *trans*-conformer but not for the *cis*-conformer. Both configurations also give a positive value for $\partial A_\mu / \partial T$ at ambient temperature as seen experimentally. Interestingly though, the *trans*-conformer is predicted to have a negative $\partial A_\mu / \partial T$ at temperatures below about 120 K.

The stable configuration of the *cis*-conformer corresponds to $\theta \sim 90^\circ$, whilst the *trans*-conformer corresponds to $\theta \sim 270^\circ$. It might therefore be expected that the form of $V(\theta)$ should be the same for the *cis*-conformer start as for the *trans*-conformer but shifted by 180°. However, this is not found to be the case, as the most stable configuration for the *cis*-conformer occurs at a different value of the O–Mu bond length and C–O–Mu bond angle to that for the *trans*-conformer. In fact, the form of $V(\theta)$ starting from the *trans*-conformer (as shown in figure 6(a)) has two nearly equal minima, whereas that from the *cis*-conformer start (figure 6(b)) has two minima that are of quite different depths. The difference between the two minima of $V(\theta)$ for the *cis*-conformer is then as expected

on the basis of the static energy minimizations, which found that the *cis*-conformer was 0.08 eV lower in energy than the *trans*-conformer. This has implications for the spectrum of eigenenergies, with the lowest level for the *cis*-conformer being considerably separated from all of the others, but not so for the *trans*-conformer. This therefore has implications for the thermal averaging procedure, with the temperature dependence of $\langle A_\mu(T)\rangle$ being weaker for the *cis*-conformer than the *trans*-conformer. This also explains why $\partial A_\mu/\partial T$ changes sign at very low temperatures for the *trans*-conformer but not the *cis*-conformer. However, in both cases, the temperature dependence is considerably less than that observed experimentally [5].

The simple twofold-barrier analysis of the experimental temperature dependence of $\langle A_\mu(T)\rangle$ suggested that the barrier to rotation was about 0.03 eV, whereas in this work it was found by direct simulation to be at least 0.225 eV. This is believed to be the main source of discrepancy in the predicted temperature dependence. The most likely origin of this is the breakdown of the rigid-rotation assumption. This assumption cannot strictly be valid, as we have already shown that the bond-stretch vibration has a large classical amplitude (of the order of 1 au) which is likely to couple to the rotational motion. The resulting coupled motion could enable the muonium to find a lower-energy route around the oxygen atom than given by the rigid rotation, which would then be more in keeping with the experimental value. This would also have the effect of coupling the *cis*- and *trans*-conformer forms of $V(\theta)$ into a single form. To treat this coupled motion properly is beyond the scope of this work, as it would require either a full 3D mapping of the energy surface around the oxygen atom, or a path-integral description of the muonium atom.

It is also possible that the discrepancy may be due to a failure of the LSD approximation and the need for a better treatment of electron correlation, as LDA/LSD approximations often fail to correctly predict the energy barrier of a chemical reaction [19].

The effect of solvent molecules in liquid ethanal, or steric hindrance from other molecules in a crystal of benzophenone, have not been included. Such effects would also influence the vibronic motion of the muonium, and therefore affect both the zero-temperature and the thermally averaged values for the hyperfine coupling constant.

5. Conclusions

We have performed a series of *ab initio* simulations of a simple organic molecule, ethanal, in the presence of muonium. We have calculated the possible stable binding sites for the muonium, the effect of bond-stretching modes on the zero-temperature hyperfine coupling constant, and the effect of bond rotation on both the zero-temperature and thermally averaged values of the hyperfine coupling constant. This work, in conjunction with our previous work on benzene [2] is sufficient to give a detailed picture of the behaviour of implanted muons in benzophenone. Benzophenone is the most likely candidate for testing the proposed muon vibrational spectroscopy technique. We conclude that the detection of muonium vibrations by this technique should be experimentally verifiable in this material.

Three stable binding sites for the muonium were found by minimizing the total energy of the system whilst relaxing all the atomic coordinates. The bond-stretching frequencies for muonium at each site have been calculated, and we find that these frequencies lie in the near IR, quite distinct from any other atomic mode. This suggests that it is possible to excite these modes in isolation. By calculating the Einstein coefficients for the vibrational excitation, we find that the spontaneous lifetime of the excited state is comparable to the lifetime of the muon. This suggests that not only is it possible to excite the vibrational state, but that it is also sufficiently long lived to have a significant effect on observable

properties. We have shown that the isotropic hyperfine parameter, which may be measured in a longitudinal-field μSR experiment, is a key observable as it has a marked increase upon vibrational excitation because of the extreme non-linear variation with bond length. The exact value depends on which of the possible binding sites the muonium occupies.

We have also considered the effects of bond rotation of the oxygen–muonium bond about the carbon–oxygen axis, as this has been proposed as the explanation of the observed temperature dependence of the hyperfine coupling constant in these materials. We find that quantum zero-point fluctuations in the bond angle have a significant effect on the zero-temperature hyperfine coupling constant. In particular, they can change the sign of the observed hyperfine coupling constant, and therefore produce reasonable agreement with experimental results. This effect also produces a positive temperature dependence as observed. However, the magnitude of this temperature dependence is considerably less than that observed. This is probably due to the neglect of coupling between vibrational and rotational motion, which is not considered in this work.

Acknowledgments

We would like to thank U Jayasooriya, S F J Cox, M McCoustra, S J Blundell and D Benton for useful discussions. This work was supported by EPSRC grants GR/J67734 and GR/K79697.

References

[1] Cox S F J 1995 *Phil. Trans. R. Soc.* A **350** 171
Cox S F J 1988 *Proc. Int. Symp. on Muons and Pions in Matter (Dubna)* (Dubna: JINR) p 153
[2] Probert M I J and Fisher A J 1996 *Chem. Phys. Lett.* **259** 271
[3] Jayasooriya U 1996 private communication
[4] Cox S F J, Geeson D A, Rhodes C J, Roduner E, Scott C A and Symons M C R 1986 *Hyperfine Interact.* **32** 763
[5] Macrae R M 1990 *Doctoral Thesis* University of Glasgow
[6] Cox S F J 1987 *J. Phys. C: Solid State Phys.* **20** 3187
[7] Patterson B D 1988 *Rev. Mod. Phys.* **60** 69
[8] Eisenstein B, Prepost R and Sachs A M 1988 *Phys. Rev.* **142** 217
[9] Hohenberg P and Kohn W 1964 *Phys. Rev.* **136** 664
[10] Kohn W and Sham L J 1965 *Phys. Rev.* **140** 1133
[11] Blöchl P 1994 *Phys. Rev.* B **50** 17 953
[12] Car R and Parrinello M 1985 *Phys. Rev. Lett.* **55** 2471
[13] Vanderbilt D 1985 *Phys. Rev.* B **41** 7892
[14] Andersen O K 1975 *Phys. Rev.* B **12** 3060
[15] Cottrell T L 1958 *The Strength of Chemical Bonds* 2nd edn (Oxford: Butterworths)
[16] Pastore G, Smargiassi E and Buda F 1991 *Phys. Rev.* A **44** 6334
[17] Tassone F, Mauri F and Car R 1994 *Phys. Rev.* B **50** 10 561
[18] Heller C and McConnell H M 1960 *J. Chem. Phys.* **32** 1535
[19] Perdew J P, Chevary J A, Vosko S H, Jackson K A, Pederson M R, Singh D J and Fiolhais C 1992 *Phys. Rev.* B **46** 6671